

Chronic active lesions in multiple sclerosis: classification, terminology, and clinical significance

Assunta Dal-Bianco , Jiwon Oh , Pascal Sati  and Martina Absinta 

Abstract: In multiple sclerosis (MS), increasing disability is considered to occur due to persistent, chronic inflammation trapped within the central nervous system (CNS). This condition, known as smoldering neuroinflammation, is present across the clinical spectrum of MS and is currently understood to be relatively resistant to treatment with existing disease-modifying therapies. Chronic active white matter lesions represent a key component of smoldering neuroinflammation. Initially characterized in autopsy specimens, multiple approaches to visualize chronic active lesions (CALs) in vivo using advanced neuroimaging techniques and postprocessing methods are rapidly emerging. Among these in vivo imaging correlates of CALs, paramagnetic rim lesions (PRLs) are defined by the presence of a perilesional rim formed by iron-laden microglia and macrophages, whereas slowly expanding lesions are identified based on linear, concentric lesion expansion over time. In recent years, several longitudinal studies have linked the occurrence of in vivo detected CALs to a more aggressive disease course. PRLs are highly specific to MS and therefore have recently been incorporated into the MS diagnostic criteria. They also have prognostic potential as biomarkers to identify patients at risk of early and severe disease progression. These developments could significantly affect MS care and the evaluation of new treatments. This review describes the latest knowledge on CAL biology and imaging and the relevance of CALs to the natural history of MS. In addition, we outline considerations for current and future in vivo biomarkers of CALs, emphasizing the need for validation, standardization, and automation in their assessment.

Keywords: chronic active lesions, MRI, multiple sclerosis, paramagnetic rim lesions, PET, slowly expanding lesions

Received: 18 August 2024; revised manuscript accepted: 18 November 2024.

Introduction

There is currently a paradigm shift in the way multiple sclerosis (MS) is viewed, evolving from a categorical group of clinically defined phenotypes to a continuum reflecting the disease's underlying biology. This shift reflects evidence that many people with MS (pwMS) continue to show clinical worsening while being treated with high-efficacy disease-modifying therapies (DMTs), which effectively minimize clinical and imaging activity reflective of relapse disease biology.^{1,2} It is now evident that at least two principal pathological processes are concurrent, one originating from

peripherally triggered inflammation combined with an open blood–brain barrier (BBB) and the other arising from persistent neuroinflammation confined behind the relatively intact BBB.²

Progressive MS (PMS) biology is thought to be driven by smoldering neuroinflammation in the brain parenchyma and meninges^{3–5} as well as related processes, including chronic oxidative injury, age-related iron accumulation, and mitochondrial dysfunction.¹ Microglia and macrophages, main components of the innate immune system, are considered key mediators of

Ther Adv Neurol Disord

2024, Vol. 17: 1–23

DOI: 10.1177/
17562864241306684

© The Author(s), 2024.
Article reuse guidelines:
sagepub.com/journals-
permissions

Correspondence to:
Assunta Dal-Bianco
Department of Neurology,
Medical University of
Vienna, Währinger Gürtel
18–20, Vienna 1090,
Austria

Comprehensive Center for
Clinical Neurosciences
and Mental Health,
Medical University of
Vienna, Vienna, Austria
[assunta.dal-bianco@
meduniwien.ac.at](mailto:assunta.dal-bianco@meduniwien.ac.at)

Jiwon Oh
Division of Neurology,
Department of Medicine,
St. Michael's Hospital,
University of Toronto,
Toronto, ON, Canada

Pascal Sati
Department of Neurology,
Cedars-Sinai Medical
Center, Los Angeles, CA,
USA

Martina Absinta
Department of Biomedical
Sciences, Humanitas
University, Milan, Italy
Experimental
Neuropathology Lab,
Neuro Center, IRCCS
Humanitas Research
Hospital, Milan, Italy

smoldering neuroinflammation and are found not only in focal demyelinating lesions but also diffusively in the normal-appearing white and gray matter.^{6,7} A key manifestation of chronic neuroinflammation in MS is reflected through chronic active lesions (CALs). The occurrence of CALs is suggested to impede tissue repair mechanisms, resulting in substantial intralesional and perilesional tissue damage.⁸ CAL-associated tissue damage also contributes to sustained neuroinflammation and is thought to be mediated by microglia and macrophages via the release of inflammatory mediators.⁸

This review describes current knowledge surrounding CALs, explores the potential implications from preliminary studies regarding the clinical applicability of CAL imaging modalities, and identifies obstacles and opportunities in the routine clinical assessment of CALs.

Biological basis of CALs

In seminal autopsy studies, CALs were identified in 78% of postmortem specimens obtained from pwMS, accounting for about 30% of total lesions.^{9,10} While these initial autopsy studies noted a higher prevalence of CALs in people with PMS than with relapsing-remitting MS (RRMS),^{9,10} recent *in vivo* studies have demonstrated that CALs manifest across the entire MS disease continuum.^{11–16} CALs have been detected in supratentorial and infratentorial regions of the brain and in the spinal cord.⁹

Histopathologically, CALs are characterized by a demyelinated core with axonal loss and an inflammatory demyelinating lesion edge (Figure 1).^{10,17} At the CAL edge, smoldering inflammation and centrifugal tissue injury are linked to the presence of microglia and macrophages (Supplemental Figure S1), which may contain myelin degradation products.¹¹ Aggregation of myeloid cells at the CAL edge was initially observed with staining for human leukocyte antigen or CD68, which does not discriminate between microglia and macrophage lineages.^{10,18} However, gene expression studies, including single-nucleus RNA-sequencing studies (Table 1), have confirmed that both microglia and macrophages are part of the detrimental inflammatory signature at the CAL edge, together with damaged oligodendrocytes, immune-like oligodendrocyte precursor cells, and activated/toxic astrocytes.^{19–21}

Chronic active white matter lesion

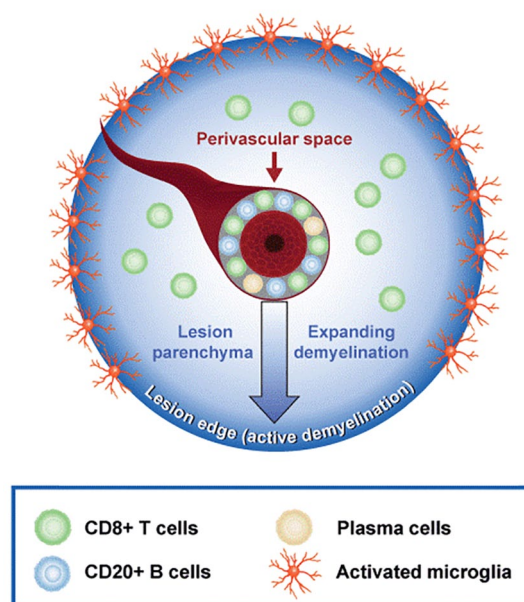


Figure 1. Evolution of a focal white matter lesion and origin of a CAL. CALs evolve from newly formed lesions behind a closed blood–brain barrier.⁸ Histopathologically, CALs feature a demyelinated core with axonal loss and an inflamed rim.^{10,11} Activated proinflammatory microglia and macrophages at the lesion rim may contain myelin degradation products, indicating ongoing demyelination.¹¹ The rim may also include damaged oligodendrocytes, activated astrocytes, and some lymphocytes.^{19–21} CAL, chronic active lesion.

Lymphocytes are sparsely present at the CAL edge, being predominantly located within the perivascular spaces and comprising mostly plasmablasts and T cells, including tissue-resident memory T cells.²²

Microglia and macrophages in CALs acquire iron, which has made *in vivo* visualization of a subtype of CALs possible. The main sources of iron accumulation are considered to be erythrocytes leaking through a minimally impaired BBB and/or disintegrated oligodendrocytes and myelin.^{18,26} The formation and dissolution of iron rims is a dynamic process involving the arrangement of iron-laden, mainly pro-inflammatory microglia and macrophages at the lesion edge, which subsequently diminish and then gradually disappear over a decade.^{19,27} The CAL rim and peri-rim area demonstrate ongoing axonal injury (i.e., presence of axonal end-bulbs) and

Table 1. Gene expression studies of CAL rims.

Recent gene expression studies have started to provide molecular insights into the processes occurring at the edge of CALs. Studies of overall gene expression from all cell types in CAL rims reported upregulation of genes related to lipid uptake and binding (e.g., *CHIT1* and *MSR1*)²⁰ as well as genes associated with metabolic processes, transcription, translation, and the MHC class II.²¹ In an analysis by cell type at CAL rims, “MIMS” displayed enrichment of pathways relevant to disease-associated phenotypes.¹⁹ Many of the genes in these pathways are related to the immune response, including *TREM2*, *APOE*, and MHC class II genes.¹⁹ The C1q was found to be a key mediator in the activation of these microglia.¹⁹ Furthermore, complement *C3AR* gene expression in MIMS, together with *C3* upregulation in “astrocytes inflamed in MS,” indicated the importance of the C3-C3AR pathway in the interaction between these cells.¹⁹ A recent study of cerebrospinal fluid intercellular communication expanded on these findings, showing that people with PRLs, compared with those without PRLs, had enrichment of C3-mediated and *SPP1*-mediated pathways.²³ *SPP1* encodes osteopontin, an extracellular matrix protein that has various effects on microglia, such as prolonging their survival.²⁴ Genes encoding osteopontin and complement factors were also found to be expressed by oligodendrocytes at the edge of CALs.²⁵ In addition, iron-related genes such as *FTH1* and *FTL* are upregulated in microglia at CAL rims, which is consistent with the importance of iron accumulation to the pathobiology at these sites.^{19,23} Of note, a recent postmortem study of people with MS reported that the CD163-HMOX1-HAMP axis was upregulated at both the RNA and protein level in myeloid cell subtypes at CAL rims, suggesting that haptoglobin-bound hemoglobin is a source of iron uptake associated with myeloid cells in MS.²⁶

C3, component 3; C3AR, component 3 receptor; CAL, chronic active lesion; MHC, major histocompatibility complex; MIMS, microglia inflamed in multiple sclerosis; MS, multiple sclerosis; PRL, paramagnetic rim lesion.

secondary retrograde axonal degeneration, known as “Wallerian degeneration.”^{8,27,28}

Imaging biomarkers of CALs

There are currently three *in vivo* imaging biomarkers of CALs: paramagnetic rim lesions (PRLs), slowly expanding lesions (SELs), and 18 kDa translocator protein (TSPO)-positron emission tomography (PET) positive lesions.

Paramagnetic rim lesions

PRLs, recently described as *in vivo* markers of CALs,^{18,27} reflect a more destructive lesion pathology compared with non-PRLs.^{8,11,28–30} Lesion-level prevalence of PRLs is ~10%, and PRLs have been observed across the spectrum of MS, with a prevalence of ~50% or more in people with clinically isolated syndrome, radiologically isolated syndrome, RRMS, and PMS.^{8,11,14–17,31–41} PRLs are specific to MS and may have clinical utility in differentiating MS from other conditions that demonstrate white-matter lesions on MRI.³⁷

The paramagnetic rims of PRLs can be identified using susceptibility-based MRI techniques (see the preceding section) and reflect the density of disease-associated iron-laden microglia and macrophages at the lesion edge.^{8,11,18,19,27} PRLs derive from a subset of acute lesions, which initially

show T1 gadolinium-enhancement on MRI with a centripetal dynamic contrast pattern, reflecting the movement of contrast across a disrupted BBB at the lesion edge, which then fills the lesion center.^{8,33} The evolution of an acute lesion into a PRL takes approximately 3 months, during which time the lesion becomes non-gadolinium-enhancing, indicating reclosure of the BBB.⁸ Prior to developing a paramagnetic rim, some PRLs initially show transient susceptibility in the lesion core, thought to reflect inflammatory activity and/or early repair mechanisms involving iron-containing oligodendrocytes.¹⁵ PRLs may persist for up to a decade as long as the iron rim has not disappeared.^{18,19,27} A disappearing rim is interpreted as the lesion transitioning toward an inactive stage. The appearance and disappearance of PRLs is related to clinical outcomes, with a recent report finding that resolution of existing rims and absence of new PRLs were associated with reduced risk of clinical disability progression.⁴²

PRLs show more pronounced tissue damage compared with non-PRLs.^{18,27} This is shown by cross-sectional observations of reduced T1 intensity (Figure 2), magnetization transfer ratio (MTR),³⁰ and increased T1 relaxation time,^{27,43} metrics that are generally indicative of decreased axonal density,⁴⁴ demyelination,⁴⁴ and microstructural tissue damage,^{45,46} respectively. Marked demyelination within the PRL core is further

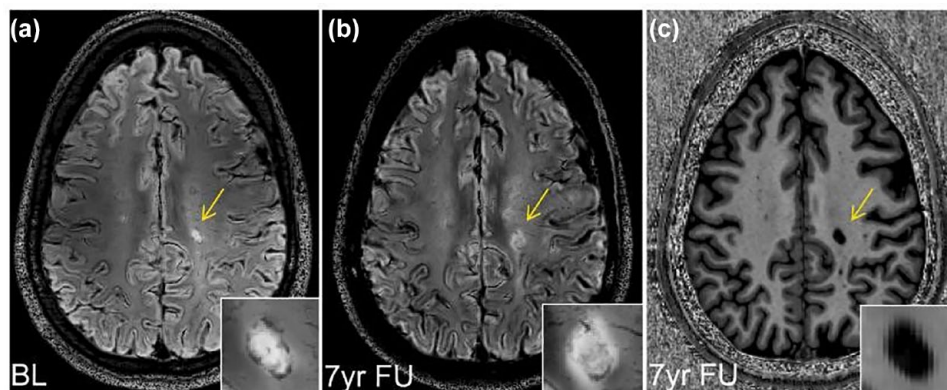


Figure 2. Longitudinal presentation of a PRL visualized using 7T FLAIR-SWI. 7T MRI scans are from a person with MS for 12 years and an MSSS of 3.94. The person is converted from RRMS to SPMS by the 7-year follow-up MRI. Panels a and b are 7T FLAIR-SWI and panel c is 7T MP2RAGE. The yellow arrows in panels a and b indicate the development of a PRL in the supratentorial white matter within 7 years enlarged in the respective bottom right corner. At baseline (a), the PRL presents as a hyperintense FLAIR lesion surrounded by an SWI-hypointense iron rim. At follow-up (b), the SWI-hypointense iron rim has diminished and is now surrounded by an evolved perilesional FLAIR hyperintensity, resulting from retrograde axonal damage (“Wallerian degeneration”). SWI-hypointense punctate or horizontal signals are also seen within this lesion, indicating veins and diffuse perivascular iron accumulation. Panel c shows marked MP2RAGE hypointensity of the PRL at 7-year follow-up, reflecting the pronounced tissue destruction of PRLs. 7T MRI scans were performed at the High-Field MR Center of the Department of Biomedical Imaging and Image-Guided Therapy, Medical University of Vienna. BL, baseline; FLAIR, fluid attenuated inversion recovery; FU, follow-up; MP2RAGE, magnetization-prepared two rapid acquisition gradient-echo; MS, multiple sclerosis; MSSS, MS Severity Score; PRL, paramagnetic rim lesion; RRMS, relapsing-remitting MS; SPMS, secondary progressive MS; SWI, susceptibility-weighted imaging; T, Tesla.

supported by the finding of a slower $R2^*$ relaxation rate versus non-PRLs.⁴³

Slowly expanding lesions

SELs have also been proposed as in vivo correlates of CALs (Figure 3),¹² since their observed short-term (typically 1–2 years) expansion is associated with ongoing microstructural lesion damage with a centrifugal pattern.^{12,47–50} This damage is suggested to occur behind the closed BBB, as SELs do not exhibit gadolinium-contrast enhancement.¹² SELs have been detected in both PMS (99% had ≥ 1 definite SEL)⁵¹ and relapsing MS (86% and 99% had ≥ 1 definite SEL and ≥ 1 possible SEL, respectively).⁵² Moreover, a larger SEL volume has been found to correspond with a higher total lesion burden.⁵¹

Compared with non-SELs, SELs show pronounced tissue damage, indicated by greater reductions in T1 intensity^{12,52} and a positive correlation with persisting black holes.⁵² Greater decreases in MTR and increases in radial diffusivity measured with diffusion tensor imaging (DTI) are found within SELs,⁴⁷ supportive of significant myelin loss.⁵² SELs also show heterogeneity in

the rate of expansion and tissue damage, with tissue loss found to be inversely proportional to the distance of the lesion from the ventricles.⁵³

Overlap of PRLs and SELs

Recently published investigations reported limited overlap between SELs and PRLs in pwMS (Figure 4), where SELs outnumbered PRLs by approximately two- to eight-fold.^{29,30} Lesions showing only PRL characteristics had more profound tissue damage at baseline compared with those featuring only SEL characteristics.³⁰ Evidence suggests that co-localized PRLs and SELs are the most destructive³⁰ and clinically unfavorable²⁹ CAL subtype according to quantitative T1 MRI, DTI, and MTR.

The presence of a paramagnetic rim may not always be associated with lesion expansion.¹⁸ Further, paramagnetic rims eventually disappear over time.²⁷ The factors that determine whether a CAL progressively expands and/or shows a paramagnetic rim are presently unclear.⁵⁴ It is currently unknown whether SELs and PRLs represent different CAL types or developmental phases. It might also be conceivable that some

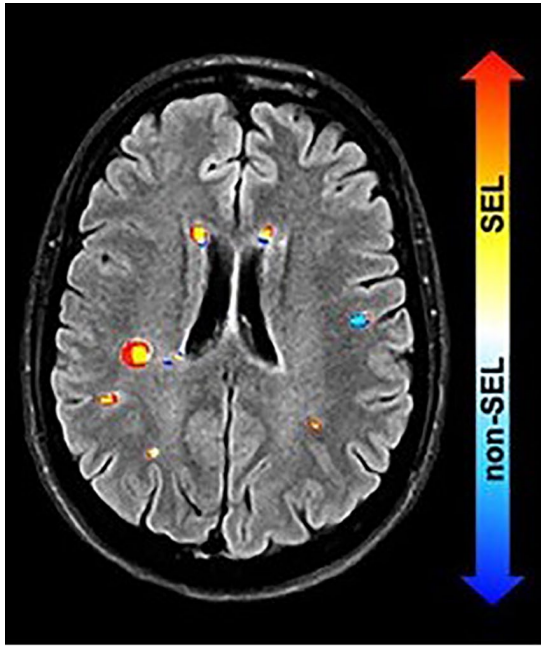


Figure 3. Slowly expanding lesions. SELs can be visualized using Jacobian analysis of the nonlinear deformation field between baseline and follow-up scans.²⁹ In this example, deformation fields were calculated from reference and follow-up T1 scans, and the Jacobian map is superimposed on a FLAIR image. The Jacobian determinant is presented as a heatmap, where blue indicates local contraction and red indicates local expansion.

Source: Calvi *et al.*²⁹ Licensed under CC BY 4.0.

FLAIR, fluid-attenuated inversion recovery; SEL, slowly expanding lesion.

SELs without a paramagnetic rim may simply contain too few iron-containing microglial cells to be detected with susceptibility-based MRI. In addition, the limited overlap between PRLs and SELs may reflect nonlinearity in the enlargement of PRLs over time, with evidence that PRL volume tends to stabilize after several years.²⁷ Nonlinear expansion is incompatible with the criteria for SELs (see the preceding section),¹² potentially inflating the rate of false-negative PRL+/SEL+ detections. For these reasons, in this review, PRLs and SELs are considered as distinct methods for visualizing a partially overlapping population of CALs whose biological processes are currently only incompletely understood.

TSPO-PET-positive lesions

CALs can be also identified with PET imaging using TSPO radioligands, which detect innate immune cells, such as microglia and macrophages that are fundamentally involved in chronic neuroinflammation (Figure 5),⁵⁰ and astrocytes.⁵⁵ While TSPO-PET signals have been reported to reflect general glial density,⁵⁵ a more recent neuropathological study found that 98% of TSPO-positive cells at the CAL edge were double positive for the microglia/macrophage markers IBA-1 and CD68, contrasting the TSPO-positive cells in inactive lesions (75%) and the center of CALs (25%) that were negative for microglia/

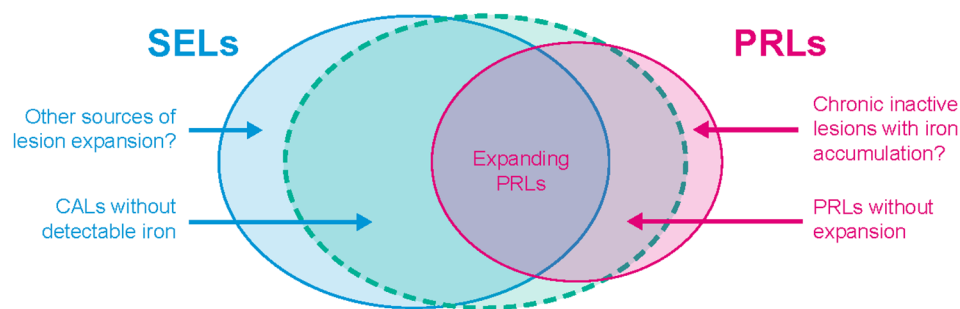


Figure 4. In vivo MRI approaches to CAL imaging. PRLs and SELs represent different MRI means of visualizing CALs.³⁰ PRLs are identified using advanced MRI techniques to detect the presence of a paramagnetic rim, which reflects iron-laden microglia/macrophages.^{18,27} SELs are detected by conventional MRI showing lesion expansion over time.^{12,50} Lesions showing characteristics of both PRLs and SELs display the most severe pathology, although overall, little overlap is observed between PRLs and SELs.³⁰

Source: Elliott *et al.*³⁰ Copyright © 2023 SAGE Publications. Reprinted by Permission of SAGE Publications.

CAL, chronic active lesion; PRL, paramagnetic rim lesion; SEL, slowly expanding lesion.

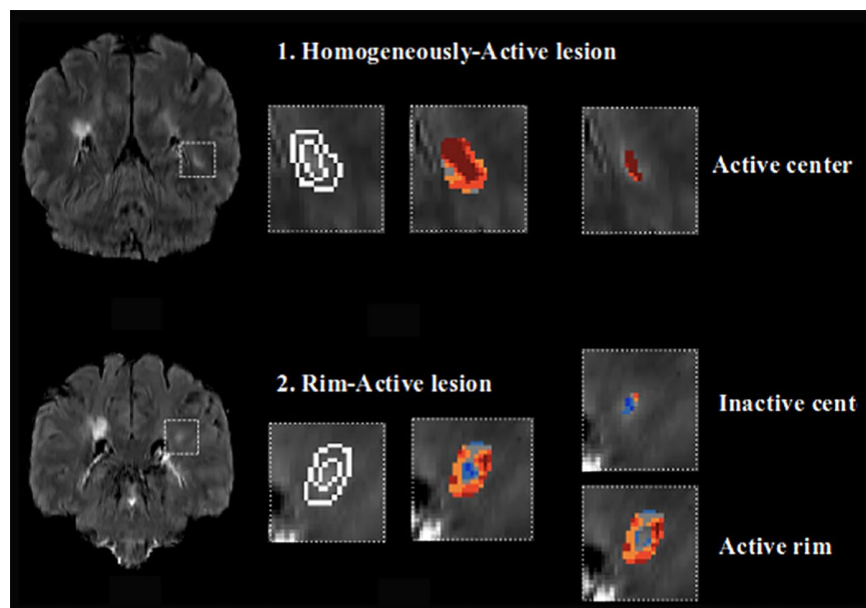


Figure 5. PET-defined CALs. Demonstration of CALs on PET in a pwMS, as defined by uptake of [18F]-DPA-714, which is a second-generation radioligand for TSPO.¹³ The TSPO-PET signal reflects microglia and macrophage density.⁵⁶ PET permits longitudinal immunological characterization of lesions,⁵⁹ and second-generation TSPO ligands differentiate MS lesions with a smoldering component from inactive lesions.¹³ In this example, the white boxes in the two illustrative MRI coronal FLAIR slices indicate lesions of interest in the white matter. The center and rim of each lesion on the FLAIR slices were delineated, and a threshold of 20% (hot colors) on the corresponding [18F]-DPA-714 PET defined areas of inflammation. Among the CALs identified in this study were (1) “homogeneously active” lesions with active centers and (2) “rim active” lesions with inactive centers and active rims.

Hamzaoui et al.¹³ Copyright © 2023 John Wiley & Sons Inc. Reproduced with permission of John Wiley & Sons Inc.

CAL, chronic active lesion; cent, center; FLAIR, fluid attenuated inversion recovery; MS, multiple sclerosis; pwMS, person with MS; TSPO, 18kDa translocator protein.

macrophage markers and presumed to be astrocytes.⁵⁶ Furthermore, a reanalysis of three single-nucleus RNA-seq studies^{19,57,58} confirms upregulation of TSPO expression in critical microglial and astrocytic inflammatory cell clusters at the CAL rim.¹³

TSPO-PET studies have identified rim-active and uniformly active chronic lesions, revealing a high proportion (48%–53%) of uniformly/homogeneously active compared to rim-active (6%–13%) and inactive (38%–41%) lesions,^{13,60} as well as an over-representation of rim-active lesions in people with secondary progressive MS (SPMS) versus RRMS (19% vs 10%; $p = 0.009$).⁶⁰ Using the first-generation TSPO radioligand [¹¹C]PK11195, the proportion of rim-active lesions (12%–16%) was consistent with the frequency of CALs reported in seminal neuropathological studies.^{9,60,61} The correspondence between rim-active lesions detected with TSPO-PET and PRLs awaits comprehensive study. One study found that, on average, PRLs detected with susceptibility-based MRI showed

greater [¹¹C]PK11195 uptake than MRI lesions without a paramagnetic rim, which was consistent with the overlapping distribution of iron and TSPO in paramagnetic rims in postmortem brain tissue.³² However, a recent study observed variable co-localization of rim-active lesions detected with TSPO-PET and PRLs.⁶²

Technological approaches and considerations for visualizing CALs

MRI is well suited to assess MS pathology in vivo.⁶³ However, conventional MRI techniques lack pathological specificity.^{64,65} There is growing interest in using advanced imaging techniques to study CALs in vivo. These MRI- and PET-based techniques evaluate CALs considering their volumetric changes, or molecular or cellular composition (Table 2). Establishing pathological specificity of CAL imaging may require further postmortem correlation studies for validation against histology, the gold standard method for identifying CALs.^{18,63,66}

Table 2. Summary of CAL imaging techniques.

Imaging technique	CAL marker	Description	Advantages	Disadvantages
Serial conventional T1- and T2-weighted MRI with Jacobian analysis	SEL	Quantifies slow concentric expansion in preexisting T2 lesions. SELs are determined through a two-step process of identifying contiguous regions of T2 lesions undergoing local expansion with Jacobian analysis, then heuristically scoring SEL candidates according to concentricity and constancy of change. ¹²	<ul style="list-style-type: none"> Derived from MRI sequences commonly used in the clinic⁶⁷ 	<ul style="list-style-type: none"> Assumes homogeneous peripheral expansion of lesions, which is inconsistent with pathological descriptions⁵⁰ Data are not directly comparable between laboratories due to use of different algorithms to detect SELs⁶⁴ Requires multiple MRI time points (at least 3 over 1–2 years)
R2* mapping	PRL	Iron produces local paramagnetic effects due to microscopic field gradients. These effects contribute to the decay of transverse magnetization observed with spoiled GRE or EPI sequences, referred to as T2* relaxation. T2* or its reciprocal R2* (1/T2*) provides a susceptibility-sensitive contrast mechanism. ^{65,68}	<ul style="list-style-type: none"> R2* maps are highly sensitive for iron, since the effect of iron content on R2* is strongly linear⁶⁹ and is increased at higher magnetic field strength⁷⁰ 	<ul style="list-style-type: none"> Iron and myelin exert counteracting effects on R2*, decreasing sensitivity to disentangle pathological changes relevant to MS⁷¹ Macroscopic susceptibility effects can produce significant signal losses as a result of dephasing along the borders between tissues with different magnetic susceptibilities, particularly at higher field strengths⁷²
Phase contrast	PRL	Local tissue susceptibility produces phase shifts in GRE and EPI images due to effects on the average magnetic field of protons in a voxel. Phase shifts relative to the surrounding tissue are either positive or negative depending on the presence of paramagnetic or diamagnetic substances, respectively. Phase data provide an excellent source of contrast to visualize susceptibility differences. ⁶⁸	<ul style="list-style-type: none"> Can be compared across studies, if echo time is held constant, since phase is independent of field strength⁷³ 	<ul style="list-style-type: none"> Uncertainties arise from the nonlocal effects of magnetic susceptibility on phase changes, which produce dipolar fields in the surrounding tissue⁷⁴; dipolar projections may impinge upon the accuracy of phase rim detection, particularly for thin ones⁷⁵ Requires phase unwrapping and high-pass filtering⁷²

(Continued)

Table 2. (Continued)

Imaging technique	CAL marker	Description	Advantages	Disadvantages
SWI	PRL	A postprocessing method that combines magnitude and phase images from a fast GRE acquisition to produce an enhanced contrast magnitude image. ⁷²	<ul style="list-style-type: none"> Greater differentiation of paramagnetic vasculature and iron deposits as compared with T2*-weighted images⁷⁶ Sensitive to very low tissue concentrations of iron⁷³ 	<ul style="list-style-type: none"> Not truly quantitative due to inclusion of an arbitrarily scaled magnitude image⁷²
QSM	PRL	A postprocessing method that removes dipole field artifacts in phase data through deconvolution. ^{32,75} Generates maps representing local variations in tissue susceptibility. ⁷⁴	<ul style="list-style-type: none"> Improved accuracy of quantification and localization of tissue iron contrast relative to other GRE-based methods^{32,40,74} Limits the effects of blooming artifacts³² Highly reproducible when same algorithm is used^{77,78} 	<ul style="list-style-type: none"> Images are generally smoothed, which can obscure fine structures, including thin paramagnetic rims⁷⁵ Multitude of QSM algorithms has been proposed. No standard has been established yet
TSPO-PET	Lesions with a rim of microglia and macrophages and a TSPO-negative center (i.e., rim-active lesions), and lesions with uniform TSPO-positivity (homogeneously active lesions) ^{13,60}	Detects the distribution of radioactivity emitted from a TSPO radioligand, most commonly [¹¹ C]PK11195. Quantifies glial cell density (>95% of TSPO-expressing cells in human white matter are microglia and macrophages). ⁵⁶	<ul style="list-style-type: none"> Permits longitudinal immunological characterization of lesions⁵⁹ 	<ul style="list-style-type: none"> Poor spatial resolution Use may be limited due to costs, required expertise, and the use of ionizing radiation⁷⁹ [¹¹C]PK11195 has suboptimal affinity, selectivity, and brain penetrance⁸⁰ (these limitations may not significantly impact clinical use) Genetic polymorphisms affect the binding of second-generation TSPO ligands⁸⁰

CAL, chronic active lesion; EPI, echo-planar imaging; GRE, gradient echo; PRL, paramagnetic rim lesion; QSM, quantitative susceptibility mapping; SEL, slowly expanding lesion; SWI, susceptibility-weighted imaging; TSPO, 18kDa translocator protein.

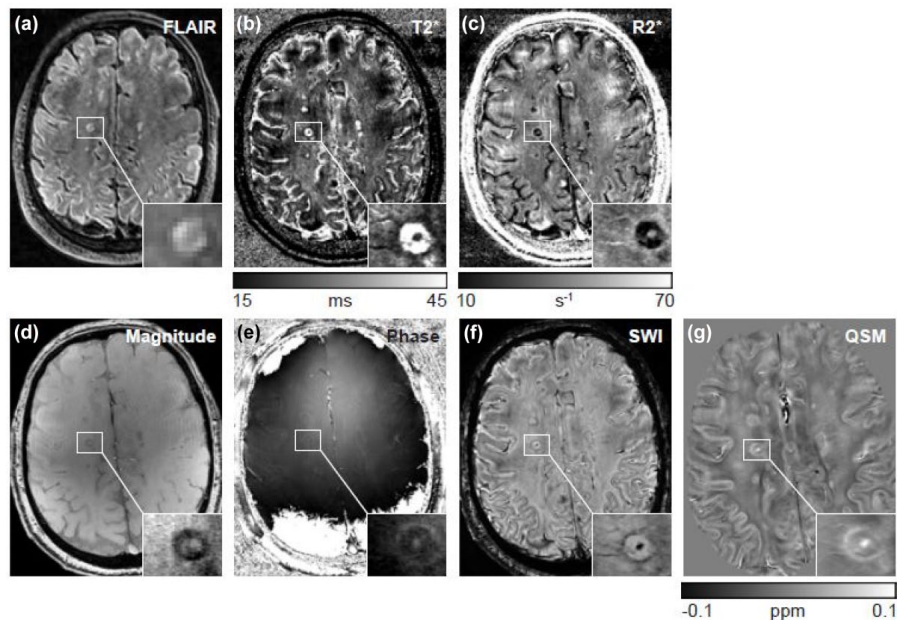


Figure 6. Example of a PRL captured with various MRI sequences. MRI scans were acquired at 7 T MRI from a 33-year-old person with RRMS for 10 years and an MS Severity Score of 0.13. The PRL is located in the supratentorial white matter of the right hemisphere and magnified in the lower right corner of each panel. Panel (a) shows the hyperintense FLAIR lesion, which presents a paramagnetic rim on T2* (b) as a hypointense signal; on R2* (c) as a hyperintense signal; on magnitude (d) as a hypointense signal; on phase (e) as a hyperintense signal; on SWI (f) as a hypointense signal; and on QSM (g) as a hyperintense signal. In addition to the rim, the lesion shows an intralésional punctate feature indicative of a central vein, as well as horizontal veins in the perilesional region. Each sequence provides unique contrast characteristics that contribute to the delineation of PRLs in MS.

Source: Images courtesy of Simon Robinson and Paul Klieber, High Field MR Centre at the Medical University of Vienna. T2* (b) and R2* (c) maps were computed from multiecho magnitude images using NumART2*.⁸⁵ Phase images (e) were generated with ASPIRE,⁸⁶ and SWI (f) using CLEAR-SWI.⁸⁷ For QSM (g), phase images were unwrapped with ROMEO⁸⁸ and background-field corrected using V-SHARP⁸⁹ prior to dipole inversion with STAR-QSM.⁹⁰ Susceptibility values were referenced to the mean, whole-brain susceptibility, all using the SEPIA interface.⁹¹

FLAIR, fluid attenuated inversion recovery; MRI, magnetic resonance imaging; MS, multiple sclerosis; ppm, parts per million; PRL, paramagnetic rim lesion; QSM, quantitative susceptibility mapping; R2*, reciprocal of T2* ($1/T2^*$); RRMS, relapsing-remitting MS; SWI, susceptibility-weighted imaging; T, Tesla; T2*, gradient echo T2-weighted imaging*.

Paramagnetic rim lesions

Susceptibility-based MRI techniques (T2* and R2*-weighted magnitude, phase images, susceptibility weighted imaging (SWI), and quantitative susceptibility mapping (QSM)) are remarkably sensitive to the magnetic properties of tissues and can evaluate both tissue microstructure and the distribution of paramagnetic substances, such as iron, and diamagnetic substances, such as myelin.^{17,81} PRLs are typically characterized as non-enhancing lesions with a distinct paramagnetic border, visible on susceptibility-based MRI, around a lesion core.⁸² Several susceptibility-based brain MRI sequences and postprocessing techniques have been used to study PRLs (Table 2; Figure 6).⁸² PRLs were first identified with 7-T MRI,⁸³ which has higher sensitivity for detecting

tissue susceptibility effects than 3 T MRI.⁷⁵ Nevertheless, identification of PRLs at 3 and 1.5 T was found to be comparable (Supplemental Figure S2), supporting the feasibility of PRL detection for trials conducted in routine clinical settings given that 1.5 T is the current global standard for clinical imaging in nonacademic settings.^{27,37,39,75,84} Also, according to the North American Imaging in MS (NAIMS) Cooperative criteria (Table 3), MRI scanners with 1.5 T or higher magnetic field strength are recommended for reliable detection of PRLs.

A single-echo GRE (gradient echo) sequence was first used to visualize PRLs in 7 T phase images.⁸³ Subsequent studies observed PRLs in the magnitude images from single-echo and multiecho

Table 3. Guidance from the NAIMS Cooperative Consensus Statement for the radiological definition of white matter PRLs.⁸²

Features of the PRL rim	<ul style="list-style-type: none"> • A distinct border displaying paramagnetic properties in a susceptibility-sensitive MRI sequence of 1.5 T or higher, exhibiting continuity along a minimum of two-thirds of the outer edge of the white matter area of the lesion (excluding any cortical or ependymal margins) within the slice of maximum visibility • The rim aligns with the border of either the entirety or a portion of a lesion core showing hyperintensity on T2-weighted images. For large T2 lesions, identifying the PRL core may be facilitated by additionally examining a more distinct hypointense core on T1-weighted images^a • The rim, either wholly or partially, is perceptible across a minimum of two consecutive slices in 2D acquisition or in two orthogonal planes in 3D acquisition
Features of the PRL core	<ul style="list-style-type: none"> • Co-localizes with the entirety or a portion of a T2-hyperintense lesion lacking enhancement on T1-weighted post-Gd-based contrast agent MRI^b
Exclusion criteria	Veins adjacent to the lesion edge that may resemble a rim
Red flags and cautions ^c	<ul style="list-style-type: none"> • Small structures exhibiting paramagnetic/diamagnetic properties, such as iron-laden ferritin or hemosiderin dots, veins, and myelin debris. However, these features may also be present in a genuine rim • PRL core of small size (e.g., diameter <3 mm in its largest dimension) • Rim thickness exceeding 2 mm (particularly applicable to phase maps, where the susceptibility alterations observed within the lesion core cannot be differentiated from those observed in the rim) • Lesions displaying magnetic dipole artifacts (often more evident in coronal or sagittal reformations) • Anatomical regions prone to susceptibility artifacts (including much of the anterior temporal lobes, orbitofrontal cortices, and infratentorial structures) • Challenges in achieving agreement in determining a PRL

^aConfluent lesions are not exempted from PRL determination provided there is a reasonable effort to distinguish an embedded PRL surrounding a distinct core.

^bIn the absence of post-Gd-based contrast agent MRI, a PRL designation should only be assigned if the corresponding lesion was detected on a T2-weighted scan acquired at least 3 (preferably 6) months earlier. If neither post-Gd-based contrast agent MRI scans nor such a prior scan are available, a PRL classification should be labeled as "possible," and its chronicity should be confirmed with a scan obtained at least 3 (preferably 6) months later.

^cItems do not necessarily rule out the classification of a lesion as a PRL.

Gd, gadolinium; NAIMS, North American Imaging in MS; PRL, paramagnetic rim lesion.

GRE scans, using maps of T2* relaxation time or its reciprocal R2* relaxivity rate,^{36,65,75,92,93} especially when iron content was higher, reflecting the lower sensitivity of T2* versus phase for tissue susceptibility effects.¹⁷ However, conventional GRE sequences are suboptimal for PRL assessment in the clinical setting because they require long acquisition times (~15–30 min) to achieve whole-brain coverage at high isotropic resolution.^{33,75} Rapid (~5 min), high-resolution susceptibility imaging of the entire brain in three planes has been achieved with a 3D segmented echo-planar imaging (3D-EPI) sequence.³⁵ 3D-EPI was optimized for the assessment of the central vein sign at 3 T MRI³⁵ but can also be applied to evaluate PRLs in the clinical setting, lowering the overall acquisition time.⁷⁵

Various postprocessing methods have been applied to facilitate PRL detection.^{34,40,94} SWI combines the complementary contrast from magnitude and phase images into one image, resulting

in improved differentiation of tissues based on paramagnetic susceptibilities.^{72,76} SWI is commonly used clinically to detect brain hemorrhage¹⁷ and has been applied for PRL detection.⁹⁴ Other postprocessing methods for PRL identification include homodyne-filtered phase images from SWI³⁴ as well as spatially unwrapped and filtered phase from standard 3D-GRE or 3D-EPI images.³³

QSM is another proposed postprocessing method that removes dipole artifacts by performing a deconvolution of phase data.^{95–97} Multiple methodologies have been proposed for QSM postprocessing,^{98–100} including recent deep learning-based techniques.^{101–104} When applied at 3 and 7 T, QSM has been shown to enable the quantification of MS brain lesions and their differentiation as PRL versus non-PRL based on their magnetic properties.^{32,40,74,77,105–110} While QSM provides a better representation of PRL geometry than phase contrast,^{40,74} use of QSM

alone to quantify iron in MS lesions is hindered by the susceptibility effects of demyelination.¹¹¹ Methods to overcome this limitation have been proposed, including combining QSM with myelin-specific imaging markers¹¹¹ and biophysical modeling to separate susceptibility sources (χ -separation).¹¹²

Given the time-consuming process of manually identifying PRLs, automatic detection methods on 3 T MRI images implementing artificial intelligence/machine learning methods have been recently proposed for both phase (i.e., RimNet,¹¹³ and APRL^{114,115}) and QSM images (i.e., QSMRim-Net¹¹⁶). While more technical development and large-scale validation studies are still needed, these initial proof-of-concept methods open the path for future deployment of automated PRL detection in the clinical setting.

PRLs have predominantly been identified in the supratentorial brain, with lesser occurrence in the infratentorial regions, although this could be due to limited brain coverage on imaging or difficulties in identifying PRLs in areas of severe susceptibility-related image artifacts. Recent advances in the use of susceptibility sequences at 7 T have provided preliminary *in vivo* evidence suggesting that PRLs may occur in the cervical spine,¹¹⁷ which has important translational implications given that spinal cord damage is clinically eloquent in MS and a predictor of future disability.¹¹⁷

Slowly expanding lesions

SELs are identified by calculating deformation fields between reference and follow-up scans using conventional MRI.¹² This analysis defines SELs as foci of constant and concentric expansion within existing T2 lesions over 1–2 years.¹² Using the Jacobian algorithm, deformation fields have been derived from serial T2-weighted images¹² or a combination of T1- and T2-weighted images,⁶⁷ with the latter providing enhanced lesion contrast and potentially increased sensitivity in detecting small changes.⁶⁷ Other methods to detect lesion expansion in serial images without Jacobian analysis have been proposed, including analysis of 3D morphological features¹¹⁸ and threshold-based detection of volume change in co-registered lesion masks.¹¹⁹ However, these alternative methods are yet to be comprehensively evaluated.

Currently, no systematic MRI-pathological study has assessed whether SELs defined by the Jacobian algorithm are indeed CALs. Pathological descriptions indicate that the centers of CALs may contract over time, potentially offsetting expansion at the lesion edge without including the whole lesion perimeter,⁹ which questions the hypothesized homogeneity of peripheral expansion.⁵⁰ It remains to be determined whether the morphology and dynamic features of SELs vary among anatomical regions and over longer follow-up periods.¹²

TSPO-PET-positive lesions

In TSPO-PET, radiolabeled TSPO ligands are administered into the peripheral circulation, which then distribute according to the tracer's pharmacokinetics and bind to TSPO in cells, including microglia and macrophages, enabling their visualization with PET.⁸⁰ With improvement in second- or third-generation TSPO ligands ([18F]DPA-714, [18F]PBR111, and [11C]PBR28) regarding greater brain penetrance, binding affinity, and target selectivity than [11C]PK11195,⁸⁰ TSPO-PET is gaining attention as an advanced imaging technique for *in vivo* phenotyping of MS lesions as homogeneously active, rim-active, or inactive, as well as for monitoring microglial-driven diffuse neuroinflammation behind the BBB.^{13,60,120} CAL activity detected with TSPO-PET shows promising correlations with clinical and MRI disease progression and cognitive function (see the preceding section),^{13,60} and has potential for clinical application in the future. For instance, TSPO-PET may have utility in solving the “clinical-radiological paradox,” where lesion burden on MRI does not always directly correlate with clinical symptoms; specifically, for some pwMS, positive TSPO-PET findings may be able to bridge the gap between stable MRI activity and worsening of clinical symptoms.

Though PET offers greater molecular specificity and different insights than MRI,⁸² several aspects of PET imaging continue to limit its clinical application to academic centers, including limited availability, high costs, technical challenges such as low intrinsic spatial resolution,⁶¹ and the complexity of data analysis^{121,122} and interpretation. Despite these challenges, chronic neuroinflammation can be reliably assessed with TSPO-PET when well-validated

postprocessing and image analysis methods are used.^{121,122}

Novel PET ligands have been developed with affinity for P2X₇ receptors,^{123,124} P2Y₁₂ receptors,¹²³ folate,¹²⁵ and colony-stimulating factor 1 receptor,¹²⁶ among others. However, it still remains to be seen whether PET imaging for non-TSPO microglial targets meaningfully improves the *in vivo* delineation of MS lesions.

Association of CALs with clinical and MRI disease progression

Neuropathological studies have shown that the number of CALs relative to total lesions is associated with the rate of disability accumulation as well as high lesion load and low remyelination.¹⁰ These findings suggest that CAL-mediated tissue injury worsens the clinical disease course. CAL imaging provides a means to investigate real-time relationships between CALs and the disease course, *in vivo*.

PwMS with PRLs more commonly present with MRI and clinical features that point to a more aggressive MS disease course than pwMS without PRLs,^{11,14,31,38,127,128} including long-term relapse rates.^{129,130} One potential caveat is that most of these studies did not control for the total MS lesion load, which is reportedly higher in the brain^{14,38,128} and spinal cord^{14,127} of pwMS with PRLs. However, studies have also reported correlations between the number of PRLs and several serum, cerebrospinal fluid (CSF), and ophthalmic biomarkers of neurodegeneration and gliosis,^{28,131–134} including levels of serum neurofilament light chain (sNfL),²⁸ plasma glial fibrillary acidic protein,¹³⁴ and CSF chitinase 3-like 1¹³³ independent of total lesion burden. An independent relationship between PRL load and sNfL levels is further supported by a study that observed this association in people with nonacute MS (no gadolinium-enhancing lesions or recent relapses), indicating ongoing axonal injury despite no evident relapse pathology.²⁸

Several studies have confirmed that the presence of PRLs is associated with increased disability cross-sectionally (as assessed by the Expanded Disability Status Scale (EDSS), MS Severity Score, Paced Auditory Serial Addition Test, pyramidal functional score, and Symbol Digit Modalities Test scores) and higher risk of

conversion from clinically isolated syndrome to MS.^{11,14,15,31,127,135,136} Even in radiologically isolated syndrome, an association between PRLs and clinical disability is evident: among various MRI measures, number of PRLs was most strongly correlated with cognitive impairment, present in one-third of the cohort.¹³⁵ Importantly, prospective cohort studies have found that the number of PRLs at baseline is associated with higher EDSS scores at follow-up, independent of variables related to the clinical phenotype; therefore, linking increased burden of focal chronic inflammatory activity with disability accumulation.^{11,15} In a separate prospective study, PRL volume was among the most important MRI variables predicting EDSS score worsening in a random forest analysis.³⁸ However, since these studies included participants with relapsing MS,^{11,15,38} the EDSS score changes predicted by PRL burden might have reflected both relapse-associated worsening and progression independent of relapse activity (PIRA). More recently, the presence of PRLs has been shown to specifically predict PIRA,^{22,137,138} with large multicenter studies finding that the occurrence of PIRA was independently associated with the baseline number of PRLs over 4 years of follow-up¹³⁷ and with the presence of >4 PRLs even already over 2 years of follow-up.¹³⁸ Recent studies have indicated that SEL volume is associated with disability accumulation.^{48,52,139} Another study found that both the proportion of SELs among white matter lesions and the MTR of SELs were independent predictors of future EDSS score worsening and that the MTR of SELs predicted RRMS to SPMS conversion.⁶⁷

The link between PRLs and more severe disease course may reflect a synergistic effect via co-localization with SELs.^{29,30} Total lesion load has been suggested to drive co-localization of SELs and PRLs.²⁹ Correlation of SELs and PRLs has been found to predict disability accumulation,²⁹ consistent with the pronounced tissue damage associated with SEL+/PRL+ lesions.³⁰ This suggests an additive effect of SELs and PRLs on chronic neuroinflammation and decreased remyelination.²⁹

Data are beginning to emerge on TSPO-PET-visualized CALs and their impact on disability accumulation and disease mechanisms. In a cross-sectional analysis of participants with rim-positive lesions observed using [¹¹C]PK11195, the number of active voxels at the rim and the

volume of rim-active lesions were associated with higher EDSS score, with the former measure also higher among SPMS compared with RRMS participants.⁶⁰ In addition, the number and volume of rim-active lesions detected with [¹¹C]PK11195 were found to be positively correlated with sNfL levels,¹⁴⁰ consistent with findings on PRLs and sNfL levels.²⁸ Longitudinal proof-of-concept studies support the usability and clinical relevance of TSPO-PET-detected CALs in predicting clinical progression.^{13,61} In one longitudinal study that used [¹¹C]PK11195, pwMS with a high proportion of rim-active lesions and a low proportion of inactive lesions were much more likely to experience EDSS progression during a 5-year follow-up than other pwMS.⁶¹ In another longitudinal study, the number of homogeneously active CALs (i.e., those with an active center), detected with [¹⁸F]-DPA-714, was found to be the strongest predictor of subsequent brain atrophy and EDSS score worsening.¹³ This growing body of evidence for CALs as drivers of neuronal damage highlights their value as potential predictors of MS disease progression and disability accumulation.

Effects of DMTs on imaging biomarkers of CALs

The application of imaging to study the effects of DMTs on the formation and structure of CALs has the potential to provide a unique perspective of treatment effects on smoldering neuroinflammation, which may be challenging to detect using conventional neurological examination.¹

Paramagnetic rim lesions

In a cross-sectional analysis, many pwMS had ≥ 1 PRL despite receiving DMTs such as dimethyl fumarate, natalizumab, fingolimod, and ocrelizumab,¹¹ indicating inadequate control of smoldering neuroinflammation with current treatments. This view is consistent with the results of several longitudinal studies,^{22,141,142} although larger cohorts and longer follow-ups are required to elucidate the long-term therapeutic effect on CALs. In one 2-year study, there was no significant treatment effect of B-cell-depleting therapy on PRL rim persistence, volume, susceptibility, or T1 times.²² In another study, dimethyl fumarate, fingolimod, and ocrelizumab showed less decrease in the T1:T2 ratio in PRLs after 2 years compared to no treatment, suggesting that DMTs may have a beneficial effect on the developing tissue

damage in PRLs,¹⁴¹ which is consistent with a study showing reduced susceptibility in PRLs with dimethyl fumarate.¹⁴³ In contrast, a recent study found that the number and volume of PRLs was stable after teriflunomide treatment for 24 months or longer.¹⁴²

Novel small-molecule DMTs designed to cross the BBB to potentially target microglia may have more direct effects on CALs. Several inhibitors of the enzyme Bruton's tyrosine kinase (BTK), which differ in their potency and ability to cross the BBB, are currently being investigated in late-stage clinical trials as potential MS treatments.¹⁴⁴ BTK is an attractive target given its important role in signaling pathways that control the activation, maturation, and survival of B cells and myeloid cells including microglia.¹⁴⁴ The potential for a brain-penetrant BTK inhibitor to affect CALs was highlighted in a recent study of autopsy tissue, which reported upregulated expression of the *Btk* gene in CALs, compared with control white matter.¹⁴⁵

Changes in the number of PRLs, as well as number and volume of SELs, are being assessed for the BTK inhibitor tolebrutinib in exploratory analyses of phase III trials (NCT04410978; NCT04410991; NCT04411641; NCT04458051) and an open-label extension (NCT03996291) of a phase IIb trial.¹⁴⁶

PRLs are being assessed as a primary end point in the phase II BRaKe MS trial (NCT04742400), in which pwMS with ≥ 1 baseline PRL switched to treatment with tolebrutinib 60 mg after at least 6 months of ocrelizumab treatment.¹⁴⁷ A recent analysis of trial data using single-cell transcriptomics identified a myeloid cell cluster in the CSF that increased, as a proportion of all myeloid cells, at 48 weeks after the switch from ocrelizumab to tolebrutinib.¹⁴⁷ Ontology analysis of genes downregulated in this cluster revealed enrichment for terms including ribosome, antigen processing and presentation, major histocompatibility complex (MHC) class II protein, extracellular exosome, phagosome, regulation of T-cell activation, and cytokine production.¹⁴⁷ Many of these genes (e.g., MHC class II genes, *APOE*, and the iron-related *FTL* and *FTH1* genes) that were downregulated after tolebrutinib treatment¹⁴⁷ were previously found to be upregulated in CAL rims¹⁹ (Table 1). Consistent with gene expression findings, BraKe

MS participants showed an altered abundance of proteins in the spinal fluid after tolebrutinib treatment, with the levels of 30 disease-associated proteins reduced after 48 weeks of tolebrutinib treatment, including NfL and the chemokine ligands CXCL10, CCL3, and CCL4.¹⁴⁸ These data are consistent with transcriptomic and proteomic changes in the CSF upon BTK inhibition, suggesting a less inflammatory and neurodegenerative profile in tolebrutinib-treated pwMS with ≥ 1 baseline PRL who switched from ocrelizumab.

Slowly expanding lesions

Recent attempts to study the effects of DMTs on the formation and structure of CALs have focused on the reanalysis of clinical trial data assessing SELs.^{48,49,139} An exploratory analysis of the phase III ORATORIO trial reported significant reductions in T1 signal intensity and T1 volume accumulation within the SELs with ocrelizumab but no effect on overall SEL prevalence.⁴⁸ Studies of natalizumab treatment on SELs have also provided mixed findings. In an exploratory analysis of the phase III ASCEND trial, natalizumab treatment was associated with a reduced prevalence of SELs and reduced T1 volume increase in SELs and non-SELs versus placebo.¹³⁹ An observational study of natalizumab and fingolimod reported modest effects for both agents on SEL-related endpoints.⁴⁹

Interpreting the effect of DMTs on SEL dynamics is challenging because the biological basis of SELs and the histopathological correlates are not fully understood. Available data indicate that current DMTs either do not have meaningful effects on SELs or have relatively modest impact, which would likely reflect predominantly indirect effects of strong peripheral anti-inflammatory action.^{48,49} Studies with longer follow-up are needed to test the hypothesis that SELs correlate with poor outcomes on disability measures. A limitation of SEL detection is that it omits CALs that may not show lesion expansion as assessed by T1- or T2-weighted MRI.¹³⁹

In the phase II trial of the BTK inhibitor evobrutinib, SEL volume after 48 weeks/end of treatment was reduced with evobrutinib 75 mg twice daily (comparator was 24 weeks of placebo followed by 24 weeks of evobrutinib 25 mg once daily), although statistical significance was not

reached when only completers at 48 weeks were assessed.¹⁴⁹ Of note, two phase III clinical trials comparing evobrutinib with teriflunomide in RMS (evolutionRMS 1 and 2) failed to meet their primary end points of reducing annualized relapse rates. Additional results are expected to be reported in the near future.

TSPO-PET-positive lesions

Analyses of rim lesions, either as PRLs or with TSPO-PET, can detect local immune cell responses as these imaging modalities have a distinct cellular correlate. The potential value of combining these approaches was demonstrated in a recent observational study of teriflunomide-treated pwMS, which reported a correlation between QSM-MRI positivity and glial density as assessed by visual inspection of TSPO-PET data.⁶² Preliminary results indicate that TSPO-PET can track changes in CALs, with studies showing a small reduction in TSPO-PET positivity in CAL rims after 1 year of natalizumab treatment.^{150,151} Future research should assess if treatment effects in CALs differ over time for TSPO-PET-positive lesions and PRLs.

Guidance from imaging groups

A recent consensus statement from the NAIMS Cooperative summarized current knowledge on imaging CALs, offering guidance for defining and implementing the three CAL imaging biomarkers.⁸² PRLs were considered the CAL biomarker with the most robust histopathological support. Accordingly, the consensus established a radiological definition of PRL to enhance standardization and facilitate future reporting of this biomarker in clinical settings (Table 3).⁸² There was agreement that SELs require a minimum of three scans, ideally over 1–2 years, and that optimization of current SEL quantification methods may result in improved markers of CAL activity. The consensus statement noted that while TSPO-PET enables improved molecular specificity to detect a wider population of CALs, the clinical feasibility of this technique is currently limited.

Clinical application of CAL biomarkers: steps and barriers

Establishment of a CAL imaging biomarker that accurately predicts disability accumulation would provide a much needed tool to evaluate

subclinical smoldering neuroinflammation in clinical settings for the purposes of prognostication, disease monitoring, patient stratification, and treatment response prediction.^{28,50} Additionally, dynamic biomarkers of CALs that correlate with disability accumulation are promising outcome measures in clinical trials of potential DMTs targeting smoldering neuroinflammation.

There are several obstacles to the translation of CAL imaging into clinical practice. The recently published NAIMS consensus statement has provided definitions of CALs based on *in vivo* imaging⁸²; however, these definitions are likely to evolve with new data. One example is the recent discovery of homogeneously active lesions by TSPO-PET, which, without neuropathological validation, have been hypothesized to represent a transition stage between late active lesions and histopathologically defined CALs.¹³ Another example is the description of juxtacortical paramagnetic rims not surrounding white matter lesions, which are associated with iron-laden microglia and cortical demyelination.¹⁵² Future studies using novel imaging techniques and post-processing methods will likely provide alternative CAL visualization methods beyond volumetric changes and composition of iron and innate immune cells.^{153–155} Preliminary work has shown initial value in differentiating CALs from other lesion types based on their higher sodium concentration,¹⁵³ rim-to-core differences in DTI-detectable tissue damage,¹⁵⁴ and textural features in T1-weighted 3D magnetization-prepared rapid acquisition gradient-echo images.¹⁵⁵

Accessibility and standardization are key requirements for the clinical use of imaging biomarkers. Acquisition protocols must be widely available on commercial scanners, while postacquisition processing should be built into imaging systems, not be overly cumbersome, and enable extraction of quantitative outputs that can be referenced against established clinically relevant or actionable cutoff values.¹⁵⁶ Standardized MRI protocols are key for PRL detection, since artifacts and signal variability can make their classification ambiguous.^{39,157} The impact of different sequences and field strengths on the accuracy and reliability of PRL detection has not been comprehensively examined,¹⁷ and QSM algorithms are not currently available on commercial scanners.¹⁵⁶ Several manufacturers offer SWI³⁹; however, current

international guidelines do not include SWI in the standard MS MRI protocol.¹⁵⁸ Issues currently limiting the implementation of SELs as a CAL biomarker include the availability of Jacobian analysis, nonstandardized detection algorithms, and a lack of consensus regarding the metrics for evaluating SEL expansion (i.e., thresholds defining meaningful lesion expansion, total SEL volume, or volume change within SELs).⁵⁴ Automated image analysis methods are necessary to assess CALs on a large scale. Manual identification of paramagnetic rims is time-consuming and subject to inter- and intrarater variability.¹⁵⁷ Several reliable machine learning methods can identify PRLs from QSM¹¹⁶ and 3D-EPI T2*-weighted and phase images,^{113,114} with QSM outperforming other methods in lesion-wise sensitivity and specificity.¹¹⁶ It is yet to be determined whether the accuracy of machine learning methods for detecting PRLs could be improved by including other PRL-specific imaging measures, such as the presence of deeply hypointense voxels on 3D T1-weighted turbo field echo.¹⁵⁹ Machine learning approaches could consider rim presence as a continuous rather than binary parameter, with intermediate values signifying ambiguity in lesion classification, but also potentially different stages of PRL evolution, reflecting the density of innate immune cells at the lesion edge.¹¹⁴

The question of which PRL detection methods are best suited for clinical practice and trials needs to consider the global availability of the method in routine clinical settings. Considering all pros and cons, phase/magnitude and SWI stand out as the most commonly available, practical, and currently most effective methods for PRL detection, striking a balance between image quality and accessibility. This recommendation ensures that availability, diagnostic utility, and cost efficiency are well aligned to meet the qualitative requirements of both routine clinical practice and global clinical trials. Although QSM is more sensitive in detecting subtle differences in magnetic susceptibility, it requires specialized software and hardware, as well as more complex postprocessing techniques, which are generally unavailable outside of universities and advanced research centers. QSM is therefore a less feasible option than phase/magnitude and SWI for PRL detection in standard clinical practice and is also not aligned with the aspiration of increasing global clinical trial participation, including from low-income countries.

Finally, appropriate training is warranted for neurologists and radiologists on the use of CAL biomarkers. Multidisciplinary partnerships between neuroradiologists and neurologists are important for accurate reading and interpretation of CAL imaging scans and translating these findings into optimum MS care. A recent systematic review concluded that there is a need for completeness in reporting factors relevant to the reliability of PRL assessment, including rater level of training and extent of experience.⁷⁷ The use of semiautomated software has been shown to enhance the accuracy of new MS lesion detection by non-neuroradiologists,¹⁶⁰ thus reinforcing the potential value of assistive software for CAL image analysis.

Conclusions

In recent years, we have seen great progress in the in vivo visualization of CALs. PRLs, SELs, and TSPO-PET-positive lesions have been proposed as three distinct imaging approaches to identify CALs in vivo since they are thought to represent certain histopathological features of CALs and are associated with disability accumulation in pwMS. Each method has particular advantages and disadvantages. Compared with SELs and TSPO-PET-positive lesions, PRLs have more robust histopathological support, enable time-saving, cross-sectional imaging, and can be visualized with widely available MRI sequences. PRLs have recently been incorporated in the 2024 revision of the McDonald Criteria¹⁶¹; therefore, representing the first CAL imaging biomarker to be integrated into routine clinical practice. Efforts to optimize imaging and postprocessing techniques as well as the application of machine learning for improved CAL detection are ongoing. With the current impetus to identify DMTs that cross the BBB and target smoldering neuroinflammation, the role of CALs in the assessment of MS prognosis, evaluation of DMT efficacy, and personalization of treatment regimens is anticipated to increase substantially. The impact of DMTs on decreasing CAL burden and the resulting effect on MS disease progression has the potential to change the MS treatment landscape. Given the focus on broad global applicability, MRI-based PRL detection remains the most feasible option for widespread clinical use to detect CALs. It is evident that there is an urgent need for susceptibility sequences, such as SWI, to be acquired as part of clinical routine to enable PRL reporting. This will require collaboration between radiologists and neurologists to ensure optimal

interpretation, especially with implementation of PRLs in the 2024 McDonald criteria.

Declarations

Ethics approval and consent to participate
Not applicable.

Consent for publication
Not applicable.

Author contributions

Assunta Dal-Bianco: Conceptualization; Methodology; Writing – review & editing.

Jiwon Oh: Conceptualization; Methodology; Writing – review & editing.

Pascal Sati: Conceptualization; Methodology; Writing – review & editing.

Martina Absinta: Conceptualization; Methodology; Writing – review & editing.

Acknowledgements

We thank Jelena Stojanovic-Radic, PhD, and Svend S. Geertsens, PhD, of Sanofi, for contributions to the planning, review, and coordination of the manuscript. Medical writing assistance was provided by Richard J. Hogan, PhD, and Conor F. Underwood, PhD, of Envision Pharma Group, and was funded by Sanofi.

Funding

The authors disclosed receipt of the following financial support for the research, authorship, and/or publication of this article: Editorial support was funded by Sanofi.

Competing interests

A.D.-B.'s position as junior group leader for Translational Morphology in Neuroscience is supported by a research grant from Biogen. She has participated in meetings sponsored by and received speaker honoraria or travel funding from A-med, Biogen, Celgene (BMS), GlaxoSmithKline, Janssen Austria, Merck, Novartis, Roche, Sandoz, Sanofi, and Zentiva. In addition, she has received unrestricted grants from F. Hoffmann-La Roche Ltd. and Merck GmbH, an affiliate of Merck KGaA. J.O. has received research support from the Waugh Family Chair in MS Research of the University of Toronto, MS Canada, Brain Canada, National

MS Society, National Institutes of Health, Biogen Idec, Roche, and EMD Serono. She has received personal compensation for consulting or speaking from Biogen Idec, EMD Serono, Eli Lilly and Company, Horizon Therapeutics, Novartis, Roche, and Sanofi. P.S. has received research support from the Erwin Rautenberg Foundation, National Institutes of Health, US Department of Defense, and the National MS Society. M.A. has received research support from the Conrad N. Hilton Foundation, National MS Society, Fondazione Italiana Sclerosi Multipla (FISM), International Progressive MS Alliance, Fondazione Regionale per la Ricerca Biomedica (FRRB), Roche Foundation, and Cariplo Foundation. She has received speaker and/or consultancy honoraria from Abata Therapeutics, Immunic Therapeutics, Biogen, GlaxoSmithKline, Roche, and Sanofi.


Availability of data and materials

Not applicable.

ORCID iDs

Assunta Dal-Bianco  <https://orcid.org/0000-0002-4284-3335>

Jiwon Oh  <https://orcid.org/0000-0001-5519-6088>

Pascal Sati  <https://orcid.org/0000-0002-6763-0125>

Martina Absinta  <https://orcid.org/0000-0003-0276-383X>

Supplemental material

Supplemental material for this article is available online.

References

- Giovannoni G, Popescu V, Wuerfel J, et al. Smouldering multiple sclerosis: the “real MS.” *Ther Adv Neurol Disord* 2022; 15: 17562864211066751.
- Kuhlmann T, Moccia M, Coetzee T, et al. Multiple sclerosis progression: time for a new mechanism-driven framework. *Lancet Neurol* 2023; 22: 78–88.
- Absinta M, Lassmann H and Trapp BD. Mechanisms underlying progression in multiple sclerosis. *Curr Opin Neurol* 2020; 33: 277–285.
- Magliozzi R, Howell OW, Calabrese M, et al. Meningeal inflammation as a driver of cortical grey matter pathology and clinical progression in multiple sclerosis. *Nat Rev Neurol* 2023; 19: 461–476.
- Magliozzi R, Howell O, Vora A, et al. Meningeal B-cell follicles in secondary progressive multiple sclerosis associate with early onset of disease and severe cortical pathology. *Brain* 2007; 130: 1089–1104.
- Zrzavy T, Hametner S, Wimmer I, et al. Loss of “homeostatic” microglia and patterns of their activation in active multiple sclerosis. *Brain* 2017; 140: 1900–1913.
- Lassmann H. Pathogenic mechanisms associated with different clinical courses of multiple sclerosis. *Front Immunol* 2019; 9: 3116.
- Absinta M, Sati P, Schindler M, et al. Persistent 7-tesla phase rim predicts poor outcome in new multiple sclerosis patient lesions. *J Clin Invest* 2016; 126: 2597–2609.
- Frischer JM, Weigand SD, Guo Y, et al. Clinical and pathological insights into the dynamic nature of the white matter multiple sclerosis plaque. *Ann Neurol* 2015; 78: 710–721.
- Luchetti S, Franssen NL, van Eden CG, et al. Progressive multiple sclerosis patients show substantial lesion activity that correlates with clinical disease severity and sex: a retrospective autopsy cohort analysis. *Acta Neuropathol* 2018; 135: 511–528.
- Absinta M, Sati P, Masuzzo F, et al. Association of chronic active multiple sclerosis lesions with disability in vivo. *JAMA Neurol* 2019; 76: 1474–1483.
- Elliott C, Wolinsky JS, Hauser SL, et al. Slowly expanding/evolving lesions as a magnetic resonance imaging marker of chronic active multiple sclerosis lesions. *Mult Scler* 2019; 25: 1915–1925.
- Hamzaoui M, Garcia J, Boffa G, et al. Positron emission tomography with [(18) F]-DPA-714 unveils a smoldering component in most multiple sclerosis lesions which drives disease progression. *Ann Neurol* 2023; 94: 366–383.
- Weber CE, Krämer J, Wittayer M, et al. Association of iron rim lesions with brain and cervical cord volume in relapsing multiple sclerosis. *Eur Radiol* 2022; 32: 2012–2022.
- Blindenbacher N, Brunner E, Asseyer S, et al. Evaluation of the “ring sign” and the “core sign” as a magnetic resonance imaging marker of disease activity and progression in clinically isolated syndrome and early multiple sclerosis. *Mult Scler J Exp Transl Clin* 2020; 6: 2055217320915480.

16. Suthiphosuwana S, Sati P, Absinta M, et al. Paramagnetic rim sign in radiologically isolated syndrome. *JAMA Neurol* 2020; 77: 653–655.
17. Martire MS, Moiola L, Rocca MA, et al. What is the potential of paramagnetic rim lesions as diagnostic indicators in multiple sclerosis? *Expert Rev Neurother* 2022; 22: 829–837.
18. Dal-Bianco A, Grabner G, Kronnerwetter C, et al. Slow expansion of multiple sclerosis iron rim lesions: pathology and 7 T magnetic resonance imaging. *Acta Neuropathol* 2017; 133: 25–42.
19. Absinta M, Maric D, Gharagozloo M, et al. A lymphocyte-microglia-astrocyte axis in chronic active multiple sclerosis. *Nature* 2021; 597: 709–714.
20. Hendrickx DAE, van Scheppingen J, van der Poel M, et al. Gene expression profiling of multiple sclerosis pathology identifies early patterns of demyelination surrounding chronic active lesions. *Front Immunol* 2017; 8: 1810.
21. Jäckle K, Zeis T, Schaeren-Wiemers N, et al. Molecular signature of slowly expanding lesions in progressive multiple sclerosis. *Brain* 2020; 143: 2073–2088.
22. Maggi P, Bulcke CV, Pedrini E, et al. B cell depletion therapy does not resolve chronic active multiple sclerosis lesions. *EBioMedicine* 2023; 94: 104701.
23. Raza SA, Enose-Akahata Y, Lin J-P, et al. Cerebrospinal fluid cellular transcriptome profiling and intercellular communication inference suggest dysfunctional SPP1 pathway underlying chronic active lesions in multiple sclerosis. *Mult Scler* 2023; 29(3 Suppl): O031.
24. Rosmus DD, Lange C, Ludwig F, et al. The role of osteopontin in microglia biology: current concepts and future perspectives. *Biomedicine* 2022; 10(4): 840.
25. Elkjaer ML, Hartebrodt A, Oubounyt M, et al. A single cell multi-omics map of cell type specific mechanistic drivers of multiple sclerosis lesions. *Mult Scler* 2023; 29(3 Suppl): P519.
26. Hofmann A, Krajnc N, Dal-Bianco A, et al. Myeloid cell iron uptake pathways and paramagnetic rim formation in multiple sclerosis. *Acta Neuropathol* 2023; 146: 707–724.
27. Dal-Bianco A, Grabner G, Kronnerwetter C, et al. Long-term evolution of multiple sclerosis iron rim lesions in 7 T MRI. *Brain* 2021; 144: 833–847.
28. Maggi P, Kuhle J, Schädelin S, et al. Chronic white matter inflammation and serum neurofilament levels in multiple sclerosis. *Neurology* 2021; 97: e543–e553.
29. Calvi A, Clarke MA, Prados F, et al. Relationship between paramagnetic rim lesions and slowly expanding lesions in multiple sclerosis. *Mult Scler* 2023; 29: 352–362.
30. Elliott C, Rudko DA, Arnold DL, et al. Lesion-level correspondence and longitudinal properties of paramagnetic rim and slowly expanding lesions in multiple sclerosis. *Mult Scler* 2023; 29: 680–690.
31. Marcille M, Hurtado Rúa S, Tyshkov C, et al. Disease correlates of rim lesions on quantitative susceptibility mapping in multiple sclerosis. *Sci Rep* 2022; 12: 4411.
32. Kaunzner UW, Kang Y, Zhang S, et al. Quantitative susceptibility mapping identifies inflammation in a subset of chronic multiple sclerosis lesions. *Brain* 2019; 142: 133–145.
33. Absinta M, Sati P, Gaitán MI, et al. Seven-tesla phase imaging of acute multiple sclerosis lesions: a new window into the inflammatory process. *Ann Neurol* 2013; 74: 669–678.
34. Grabner G, Dal-Bianco A, Schernthaner M, et al. Analysis of multiple sclerosis lesions using a fusion of 3.0 T FLAIR and 7.0 T SWI phase: FLAIR SWI. *J Magn Reson Imaging* 2011; 33: 543–549.
35. Sati P, Thomasson DM, Li N, et al. Rapid, high-resolution, whole-brain, susceptibility-based MRI of multiple sclerosis. *Mult Scler* 2014; 20: 1464–1470.
36. Yao B, Bagnato F, Matsuura E, et al. Chronic multiple sclerosis lesions: characterization with high-field-strength MR imaging. *Radiology* 2012; 262: 206–215.
37. Maggi P, Sati P, Nair G, et al. Paramagnetic rim lesions are specific to multiple sclerosis: an international multicenter 3T MRI study. *Ann Neurol* 2020; 88: 1034–1042.
38. Treaba CA, Conti A, Klawiter EC, et al. Cortical and phase rim lesions on 7 T MRI as markers of multiple sclerosis disease progression. *Brain Commun* 2021; 3: fcab134.
39. Hemond CC, Reich DS and Dundamadappa SK. Paramagnetic rim lesions in multiple sclerosis: comparison of visualization at 1.5-T and 3-T MRI. *AJR Am J Roentgenol* 2022; 219: 120–131.
40. Huang W, Sweeney EM, Kaunzner UW, et al. Quantitative susceptibility mapping versus phase

- imaging to identify multiple sclerosis iron rim lesions with demyelination. *J Neuroimaging* 2022; 32: 667–675.
41. Ng Kee Kwong KC, Mollison D, Meijboom R, et al. The prevalence of paramagnetic rim lesions in multiple sclerosis: a systematic review and meta-analysis. *PLoS One* 2021; 16: e0256845.
 42. Reeves JA, Bartnik A, Jakimovski D, et al. Associations between paramagnetic rim lesion evolution and clinical and radiologic disease progression in persons with multiple sclerosis. *Neurology* 2024; 103: e210004.
 43. Choi S, Lake S and Harrison DM. Evaluation of the blood-brain barrier, demyelination, and neurodegeneration in paramagnetic rim lesions in multiple sclerosis on 7 Tesla MRI. *J Magn Reson Imaging* 2024; 59: 941–951.
 44. Kolb H, Absinta M, Beck ES, et al. 7T MRI differentiates remyelinated from demyelinated multiple sclerosis lesions. *Ann Neurol* 2021; 90: 612–626.
 45. Vanden Bulcke C, Stölting A, Maric D, et al. Comparative overview of multi-shell diffusion MRI models to characterize the microstructure of multiple sclerosis lesions and periplaques. *Neuroimage Clin* 2024; 42: 103593.
 46. Rahmanzadeh R, Lu PJ, Barakovic M, et al. Myelin and axon pathology in multiple sclerosis assessed by myelin water and multi-shell diffusion imaging. *Brain* 2021; 144: 1684–1696.
 47. Elliott C, Arnold DL, Chen H, et al. Patterning chronic active demyelination in slowly expanding/evolving white matter MS lesions. *AJNR Am J Neuroradiol* 2020; 41: 1584–1591.
 48. Elliott C, Belachew S, Wolinsky JS, et al. Chronic white matter lesion activity predicts clinical progression in primary progressive multiple sclerosis. *Brain* 2019; 142: 2787–2799.
 49. Preziosa P, Pagani E, Moiola L, et al. Occurrence and microstructural features of slowly expanding lesions on fingolimod or natalizumab treatment in multiple sclerosis. *Mult Scler* 2021; 27: 1520–1532.
 50. Calvi A, Haider L, Prados F, et al. In vivo imaging of chronic active lesions in multiple sclerosis. *Mult Scler* 2022; 28: 683–690.
 51. Calvi A, Carrasco FP, Tur C, et al. Association of slowly expanding lesions on MRI with disability in people with secondary progressive multiple sclerosis. *Neurology* 2022; 98: e1783–e1793.
 52. Calvi A, Tur C, Chard D, et al. Slowly expanding lesions relate to persisting black-holes and clinical outcomes in relapse-onset multiple sclerosis. *Neuroimage Clin* 2022; 35: 103048.
 53. Klistorner S, Barnett MH, Graham SL, et al. The expansion and severity of chronic MS lesions follows a periventricular gradient. *Mult Scler* 2022; 28: 1504–1514.
 54. Simmons SB and Ontaneda D. Slowly expanding lesions: a new target for progressive multiple sclerosis trials? *Neurology* 2022; 98: 699–700.
 55. Nutma E, Stephenson JA, Gorter RP, et al. A quantitative neuropathological assessment of translocator protein expression in multiple sclerosis. *Brain* 2019; 142: 3440–3455.
 56. Nutma E, Gebro E, Marzin MC, et al. Activated microglia do not increase 18 kDa translocator protein (TSPO) expression in the multiple sclerosis brain. *Glia* 2021; 69: 2447–2458.
 57. Jäkel S, Agirre E, Mendanha Falcão A, et al. Altered human oligodendrocyte heterogeneity in multiple sclerosis. *Nature* 2019; 566: 543–547.
 58. Schirmer L, Velmeshev D, Holmqvist S, et al. Neuronal vulnerability and multilineage diversity in multiple sclerosis. *Nature* 2019; 573: 75–82.
 59. Airas L, Rissanen E and Rinne J. Imaging of microglial activation in MS using PET: research use and potential future clinical application. *Mult Scler* 2017; 23: 496–504.
 60. Nylund M, Sucksdorff M, Matilainen M, et al. Phenotyping of multiple sclerosis lesions according to innate immune cell activation using 18 kDa translocator protein-PET. *Brain Commun* 2022; 4: fcab301.
 61. Polvinen E, Matilainen M, Nylund M, et al. TSPO-detectable chronic active lesions predict disease progression in multiple sclerosis. *Neurol Neuroimmunol Neuroinflamm* 2023; 10: e200133.
 62. Lehto J, Nylund M, Matilainen M, et al. Longitudinal stability of progression-related microglial activity during teriflunomide treatment in patients with multiple sclerosis. *Eur J Neurol* 2023; 30: 2365–2375.
 63. Filippi M, Brück W, Chard D, et al. Association between pathological and MRI findings in multiple sclerosis. *Lancet Neurol* 2019; 18: 198–210.
 64. Arnold DL, Belachew S, Gafson AR, et al. Slowly expanding lesions are a marker of progressive MS—no. *Mult Scler* 2021; 27: 1681–1683.
 65. Bagnato F, Hametner S, Yao B, et al. Tracking iron in multiple sclerosis: a combined imaging

- and histopathological study at 7 Tesla. *Brain* 2011; 134: 3602–3615.
66. Preziosa P, Filippi M and Rocca MA. Chronic active lesions: a new MRI biomarker to monitor treatment effect in multiple sclerosis? *Expert Rev Neurother* 2021; 21: 837–841.
 67. Preziosa P, Pagani E, Meani A, et al. Slowly expanding lesions predict 9-year multiple sclerosis disease progression. *Neurol Neuroimmunol Neuroinflamm* 2022; 9: e1139.
 68. Chavhan GB, Babyn PS, Thomas B, et al. Principles, techniques, and applications of T2*-based MR imaging and its special applications. *Radiographics* 2009; 29: 1433–1449.
 69. Langkammer C, Krebs N, Goessler W, et al. Quantitative MR imaging of brain iron: a postmortem validation study. *Radiology* 2010; 257: 455–462.
 70. Bagnato F, Hametner S, Boyd E, et al. Untangling the R2* contrast in multiple sclerosis: a combined MRI-histology study at 7.0 Tesla. *PLoS One* 2018; 13: e0193839.
 71. Langkammer C, Liu T, Khalil M, et al. Quantitative susceptibility mapping in multiple sclerosis. *Radiology* 2013; 267: 551–559.
 72. Ropele S, de Graaf W, Khalil M, et al. MRI assessment of iron deposition in multiple sclerosis. *J Magn Reson Imaging* 2011; 34: 13–21.
 73. Haacke EM, Makki M, Ge Y, et al. Characterizing iron deposition in multiple sclerosis lesions using susceptibility weighted imaging. *J Magn Reson Imaging* 2009; 29: 537–544.
 74. Cronin MJ, Wharton S, Al-Radaideh A, et al. A comparison of phase imaging and quantitative susceptibility mapping in the imaging of multiple sclerosis lesions at ultrahigh field. *MAGMA* 2016; 29: 543–557.
 75. Absinta M, Sati P, Fechner A, et al. Identification of chronic active multiple sclerosis lesions on 3T MRI. *AJNR Am J Neuroradiol* 2018; 39: 1233–1238.
 76. Haacke EM, Mittal S, Wu Z, et al. Susceptibility-weighted imaging: technical aspects and clinical applications, part 1. *AJNR Am J Neuroradiol* 2009; 30: 19–30.
 77. Reeves JA, Mohebbi M, Zivadinov R, et al. Reliability of paramagnetic rim lesion classification on quantitative susceptibility mapping (QSM) in people with multiple sclerosis: single-site experience and systematic review. *Mult Scler Relat Disord* 2023; 79: 104968.
 78. Deh K, Nguyen TD, Eskreis-Winkler S, et al. Reproducibility of quantitative susceptibility mapping in the brain at two field strengths from two vendors. *J Magn Reson Imaging* 2015; 42: 1592–1600.
 79. Bagnato F, Gauthier SA, Laule C, et al. Imaging mechanisms of disease progression in multiple sclerosis: beyond brain atrophy. *J Neuroimaging* 2020; 30: 251–266.
 80. Viviano M, Barresi E, Siméon FG, et al. Essential principles and recent progress in the development of TSPO PET ligands for neuroinflammation imaging. *Curr Med Chem* 2022; 29: 4862–4890.
 81. Fiscone C, Rundo L, Lugaesi A, et al. Assessing robustness of quantitative susceptibility-based MRI radiomic features in patients with multiple sclerosis. *Sci Rep* 2023; 13: 16239.
 82. Bagnato F, Sati P, Hemond CC, et al. Imaging chronic active lesions in multiple sclerosis: a consensus statement. *Brain* 2024; 147: 2913–2933.
 83. Hammond KE, Metcalf M, Carvajal L, et al. Quantitative in vivo magnetic resonance imaging of multiple sclerosis at 7 Tesla with sensitivity to iron. *Ann Neurol* 2008; 64: 707–713.
 84. Ng Kee Kwong KC, Mollison D, Meijboom R, et al. Rim lesions are demonstrated in early relapsing-remitting multiple sclerosis using 3 T-based susceptibility-weighted imaging in a multi-institutional setting. *Neuroradiology* 2022; 64: 109–117.
 85. Hagberg GE, Indovina I, Sanes JN, et al. Real-time quantification of T(2)(*) changes using multiecho planar imaging and numerical methods. *Magn Reson Med* 2002; 48: 877–882.
 86. Eckstein K, Dymerska B, Bachrata B, et al. Computationally efficient combination of multi-channel phase data from Multi-echo Acquisitions (ASPIRE). *Magn Reson Med* 2018; 79: 2996–3006.
 87. Eckstein K, Bachrata B, Hangel G, et al. Improved susceptibility weighted imaging at ultra-high field using bipolar multi-echo acquisition and optimized image processing: CLEAR-SWI. *Neuroimage* 2021; 237: 118175.
 88. Dymerska B, Eckstein K, Bachrata B, et al. Phase unwrapping with a rapid opensource minimum spanning tree algorithm (ROMEO). *Magn Reson Med* 2021; 85: 2294–2308.
 89. Wu B, Li W, Guidon A, et al. Whole brain susceptibility mapping using compressed sensing. *Magn Reson Med* 2012; 67: 137–147.

90. Wei H, Dibb R, Zhou Y, et al. Streaking artifact reduction for quantitative susceptibility mapping of sources with large dynamic range. *NMR Biomed* 2015; 28: 1294–1303.
91. Chan KS and Marques JP. SEPIA-Susceptibility mapping pipeline tool for phase images. *Neuroimage* 2021; 227: 117611.
92. Pitt D, Boster A, Pei W, et al. Imaging cortical lesions in multiple sclerosis with ultra-high-field magnetic resonance imaging. *Arch Neurol* 2010; 67: 812–818.
93. Bian W, Harter K, Hammond-Rosenbluth KE, et al. A serial in vivo 7T magnetic resonance phase imaging study of white matter lesions in multiple sclerosis. *Mult Scler* 2013; 19: 69–75.
94. Eisele P, Fischer K, Szabo K, et al. Characterization of contrast-enhancing and non-contrast-enhancing multiple sclerosis lesions using susceptibility-weighted imaging. *Front Neurol* 2019; 10: 1082.
95. Wang Y, Spincemaille P, Liu Z, et al. Clinical quantitative susceptibility mapping (QSM): biometal imaging and its emerging roles in patient care. *J Magn Reson Imaging* 2017; 46: 951–971.
96. Schweser F, Deistung A and Reichenbach JR. Foundations of MRI phase imaging and processing for quantitative susceptibility mapping (QSM). *Z Med Phys* 2016; 26: 6–34.
97. Wang Y and Liu T. Quantitative susceptibility mapping (QSM): decoding MRI data for a tissue magnetic biomarker. *Magn Reson Med* 2015; 73: 82–101.
98. Bilgic B, Langkammer C, Marques JP, et al. QSM reconstruction challenge 2.0: design and report of results. *Magn Reson Med* 2021; 86: 1241–1255.
99. Milovic C, Tejos C, Acosta-Cabronero J, et al. The 2016 QSM Challenge: lessons learned and considerations for a future challenge design. *Magn Reson Med* 2020; 84: 1624–1637.
100. Jung W, Bollmann S and Lee J. Overview of quantitative susceptibility mapping using deep learning: current status, challenges and opportunities. *NMR Biomed* 2022; 35: e4292.
101. Feng R, Zhao J, Wang H, et al. MoDL-QSM: model-based deep learning for quantitative susceptibility mapping. *Neuroimage* 2021; 240: 118376.
102. Wang Z, Xia P, Huang F, et al. A data-driven deep learning pipeline for quantitative susceptibility mapping (QSM). *Magn Reson Imaging* 2022; 88: 89–100.
103. Wang Z, Mak HK and Cao P. Deep learning-regularized, single-step quantitative susceptibility mapping quantification. *NMR Biomed* 2023; 36: e4849.
104. Cognolato F, O'Brien K, Jin J, et al. NeXtQSM-A complete deep learning pipeline for data-consistent quantitative susceptibility mapping trained with hybrid data. *Med Image Anal* 2023; 84: 102700.
105. Voon CC, Wiltgen T, Wiestler B, et al. Quantitative susceptibility mapping in multiple sclerosis: a systematic review and meta-analysis. *Neuroimage Clin* 2024; 42: 103598.
106. Wisnieff C, Ramanan S, Olesik J, et al. Quantitative susceptibility mapping (QSM) of white matter multiple sclerosis lesions: interpreting positive susceptibility and the presence of iron. *Magn Reson Med* 2015; 74: 564–570.
107. Zhang Y, Gauthier SA, Gupta A, et al. Longitudinal change in magnetic susceptibility of new enhanced multiple sclerosis (MS) lesions measured on serial quantitative susceptibility mapping (QSM). *J Magn Reson Imaging* 2016; 44: 426–432.
108. Deh K, Ponath GD, Molvi Z, et al. Magnetic susceptibility increases as diamagnetic molecules breakdown: myelin digestion during multiple sclerosis lesion formation contributes to increase on QSM. *J Magn Reson Imaging* 2018; 48: 1281–1287.
109. Li X, Harrison DM, Liu H, et al. Magnetic susceptibility contrast variations in multiple sclerosis lesions. *J Magn Reson Imaging* 2016; 43: 463–473.
110. Chen W, Gauthier SA, Gupta A, et al. Quantitative susceptibility mapping of multiple sclerosis lesions at various ages. *Radiology* 2014; 271: 183–192.
111. Yao Y, Nguyen TD, Pandya S, et al. Combining quantitative susceptibility mapping with automatic zero reference (QSM0) and myelin water fraction imaging to quantify iron-related myelin damage in chronic active MS lesions. *AJNR Am J Neuroradiol* 2018; 39: 303–310.
112. Shin HG, Lee J, Yun YH, et al. χ -separation: magnetic susceptibility source separation toward iron and myelin mapping in the brain. *Neuroimage* 2021; 240: 118371.
113. Barquero G, La Rosa F, Kebiri H, et al. RimNet: a deep 3D multimodal MRI architecture for paramagnetic rim lesion assessment in multiple sclerosis. *Neuroimage Clin* 2020; 28: 102412.

114. Lou C, Sati P, Absinta M, et al. Fully automated detection of paramagnetic rims in multiple sclerosis lesions on 3T susceptibility-based MR imaging. *Neuroimage Clin* 2021; 32: 102796.
115. Chen L, Ren Z, Clark KA, et al. Multicenter validation of automated detection of paramagnetic rim lesions on brain MRI in multiple sclerosis. *J Neuroimaging* 2024; 34: 750–757.
116. Zhang H, Nguyen TD, Zhang J, et al. QSMRim-Net: imbalance-aware learning for identification of chronic active multiple sclerosis lesions on quantitative susceptibility maps. *Neuroimage Clin* 2022; 34: 102979.
117. Clarke MA, Witt AA, Robison RK, et al. Cervical spinal cord susceptibility-weighted MRI at 7T: application to multiple sclerosis. *Neuroimage* 2023; 284: 120460.
118. Okuda DT, Moog TM, McCreary M, et al. Utility of shape evolution and displacement in the classification of chronic multiple sclerosis lesions. *Sci Rep* 2020; 10: 19560.
119. Klistorner S, Barnett MH, Yiannikas C, et al. Expansion of chronic lesions is linked to disease progression in relapsing-remitting multiple sclerosis patients. *Mult Scler* 2021; 27: 1533–1542.
120. Datta G, Colasanti A, Kalk N, et al. (11)C-PBR28 and (18)F-PBR111 detect white matter inflammatory heterogeneity in multiple sclerosis. *J Nucl Med* 2017; 58: 1477–1482.
121. Guilarte TR. TSPO in diverse CNS pathologies and psychiatric disease: a critical review and a way forward. *Pharmacol Ther* 2019; 194: 44–58.
122. Sucksdorff M, Matilainen M, Tuisku J, et al. Brain TSPO-PET predicts later disease progression independent of relapses in multiple sclerosis. *Brain* 2020; 143: 3318–3330.
123. Beaino W, Janssen B, Kooij G, et al. Purinergic receptors P2Y12R and P2X7R: potential targets for PET imaging of microglia phenotypes in multiple sclerosis. *J Neuroinflammation* 2017; 14: 259.
124. Hagens MHJ, Golla SSV, Janssen B, et al. The P2X(7) receptor tracer [(11)C]SMW139 as an in vivo marker of neuroinflammation in multiple sclerosis: a first-in man study. *Eur J Nucl Med Mol Imaging* 2020; 47: 379–389.
125. Elo P, Li XG, Liljenbäck H, et al. Folate receptor-targeted positron emission tomography of experimental autoimmune encephalomyelitis in rats. *J Neuroinflammation* 2019; 16: 252.
126. Coughlin JM, Du Y, Lesniak WG, et al. First-in-human use of (11)C-CPPC with positron emission tomography for imaging the macrophage colony-stimulating factor 1 receptor. *EJNMMI Res* 2022; 12: 64.
127. Wenzel N, Wittayer M, Weber CE, et al. Multiple sclerosis iron rim lesions are linked to impaired cervical spinal cord integrity using the T1/T2-weighted ratio. *J Neuroimaging* 2023; 33: 240–246.
128. Wittayer M, Weber CE, Kittel M, et al. Cerebrospinal fluid-related tissue damage in multiple sclerosis patients with iron rim lesions. *Mult Scler* 2023; 29: 549–558.
129. Reeves JA, Mohebby M, Wicks T, et al. Paramagnetic rim lesions predict greater long-term relapse rates and clinical progression over 10 years. *Mult Scler* 2024; 30: 535–545.
130. Reeves JA, Weinstock Z, Zivadinov R, et al. Paramagnetic rim lesions are associated with greater incidence of relapse and worse cognitive recovery following relapse. *Mult Scler* 2023; 19:103.–1038.
131. Krajnc N, Dal-Bianco A, Leutmezer F, et al. Association of paramagnetic rim lesions and retinal layer thickness in patients with multiple sclerosis. *Mult Scler* 2023; 29: 374–384.
132. Dal-Bianco A, Schranzer R, Grabner G, et al. Iron rims in patients with multiple sclerosis as neurodegenerative marker? A 7-Tesla magnetic resonance study. *Front Neurol* 2021; 12: 632749.
133. Comabella M, Clarke MA, Schaedelin S, et al. CSF chitinase 3-like 1 is associated with iron rims in patients with a first demyelinating event. *Mult Scler* 2022; 28: 71–81.
134. Schneider R, Brand-Arzamendi K, Reynold Lim T, et al. Plasma glial fibrillary acidic protein levels correlate with paramagnetic rim lesions in people with radiologically isolated syndrome. *Mult Scler* 2024; 30: 156–165.
135. Oh J, Suthiphosuwana S, Sati P, et al. Cognitive impairment, the central vein sign, and paramagnetic rim lesions in RIS. *Mult Scler* 2021; 27: 2199–2208.
136. Clarke MA, Pareto D, Pessini-Ferreira L, et al. Value of 3T susceptibility-weighted imaging in the diagnosis of multiple sclerosis. *AJNR Am J Neuroradiol* 2020; 41: 1001–1008.
137. Cagol A, Benkert P, Melie-Garcia L, et al. Association of spinal cord atrophy and brain paramagnetic rim lesions with progression independent of relapse activity in people with MS. *Neurology* 2024; 102: e207768.
138. Borrelli S, Martire MS, Stölting A, et al. Central vein sign, cortical lesions, and paramagnetic rim lesions for the diagnostic and prognostic workup

- of multiple sclerosis. *Neurol Neuroimmunol Neuroinflamm* 2024; 11: e200253.
139. Beynon V, George IC, Elliott C, et al. Chronic lesion activity and disability progression in secondary progressive multiple sclerosis. *BMJ Neurol Open* 2022; 4: e000240.
 140. Saraste M, Matilainen M, Vuorimaa A, et al. Association of serum neurofilament light with microglial activation in multiple sclerosis. *J Neurol Neurosurg Psychiatry* 2023; 94: 698–706.
 141. Eisele P, Wittayer M, Weber CE, et al. Impact of disease-modifying therapies on evolving tissue damage in iron rim multiple sclerosis lesions. *Mult Scler* 2022; 28: 2294–2298.
 142. Tan H, Li X, Li Y, et al. Real-world experience of teriflunomide in relapsing multiple sclerosis: paramagnetic rim lesions may play a role. *Front Immunol* 2024; 15: 1343531.
 143. Zinger N, Ponath G, Sweeney E, et al. Dimethyl fumarate reduces inflammation in chronic active multiple sclerosis lesions. *Neurol Neuroimmunol Neuroinflamm* 2022; 9: e1138.
 144. Krämer J, Bar-Or A, Turner TJ, et al. Bruton tyrosine kinase inhibitors for multiple sclerosis. *Nat Rev Neurol* 2023; 19: 289–304.
 145. Elkjaer ML, Waede MR, Kingo C, et al. Expression of Bruton's tyrosine kinase in different type of brain lesions of multiple sclerosis patients and during experimental demyelination. *Front Immunol* 2023; 14: 1264128.
 146. Reich DS, Arnold DL, Vermersch P, et al. Safety and efficacy of tolebrutinib, an oral brain-penetrant BTK inhibitor, in relapsing multiple sclerosis: a phase 2b, randomised, double-blind, placebo-controlled trial. *Lancet Neurol* 2021; 20: 729–738.
 147. Raza SA, Enose-Akahata Y, Lin J-P, et al. Cerebrospinal fluid myeloid modulation in patients with multiple sclerosis treated with tolebrutinib. *Mult Scler* 2023; 29(3 Suppl): O058.
 148. Blazier AS, Wirak G, Krishnaswami P, et al. Tolebrutinib can reverse multiple sclerosis-induced cerebrospinal fluid proteomic alterations. *Mult Scler* 2023; 29(3 Suppl): P645.
 149. Arnold D, Elliott C, Montalban X, et al. Effects of evobrutinib, a Bruton's tyrosine kinase inhibitor, on slowly expanding lesions: an emerging marker of chronic tissue loss in multiple sclerosis. *Neurology* 2022; 98: S14.009.
 150. Sucksdorff M, Tuisku J, Matilainen M, et al. Natalizumab treatment reduces microglial activation in the white matter of the MS brain. *Neurol Neuroimmunol Neuroinflamm* 2019; 6: e574.
 151. Nylund M, Matilainen M, Sucksdorff M, et al. Impact of natalizumab on chronic active lesions (P11-3.011). *Neurology* 2023; 100: 3046.
 152. Galbusera R, Bahn E, Weigel M, et al. Characteristics, prevalence, and clinical relevance of juxtacortical paramagnetic rims in patients with multiple sclerosis. *Neurology* 2024; 102: e207966.
 153. Eisele P, Kraemer M, Dabringhaus A, et al. Characterization of chronic active multiple sclerosis lesions with sodium (²³Na) magnetic resonance imaging—preliminary observations. *Eur J Neurol* 2021; 28: 2392–2395.
 154. Oladosu O, Liu WQ, Brown L, et al. Advanced diffusion MRI and image texture analysis detect widespread brain structural differences between relapsing-remitting and secondary progressive multiple sclerosis. *Front Hum Neurosci* 2022; 16: 944908.
 155. Weber CE, Wittayer M, Kraemer M, et al. Quantitative MRI texture analysis in chronic active multiple sclerosis lesions. *Magn Reson Imaging* 2021; 79: 97–102.
 156. Granziera C, Wuerfel J, Barkhof F, et al. Quantitative magnetic resonance imaging towards clinical application in multiple sclerosis. *Brain* 2021; 144: 1296–1311.
 157. La Rosa F, Wynen M, Al-Louzi O, et al. Cortical lesions, central vein sign, and paramagnetic rim lesions in multiple sclerosis: emerging machine learning techniques and future avenues. *Neuroimage Clin* 2022; 36: 103205.
 158. Wattjes MP, Ciccarelli O, Reich DS, et al. 2021 MAGNIMS-CMSC-NAIMS consensus recommendations on the use of MRI in patients with multiple sclerosis. *Lancet Neurol* 2021; 20: 653–670.
 159. Naval-Baudin P, Pons-Escoda A, Camins À, et al. Deeply 3D-T1-TFE hypointense voxels are characteristic of phase-rim lesions in multiple sclerosis. *Eur Radiol* 2024; 34: 1337–1345.
 160. Dahan A, Wang W, Tacey M, et al. Can medical professionals with minimal-to-no neuroradiology training monitor MS disease progression using semiautomated imaging software? *Neurology* 2016; 86: P2.151.
 161. Montalban X. Oral Presentation at Scientific Session “Revised McDonald criteria 2023”; Session 1: New diagnostic criteria. ECTRIMS, 2024.